Molecular Therapy
Nucleic Acids
Original Article

LinQURE: A novel AAV gene silencing platform that supports multi-transcript targeting for complex disorders

Irena Bočkaj,[1] Anna Moreno Garcia,[1] Pablo de Miguel Herraiz,[1] Sonay Keskin,[1] Vanessa Zancanella,[1] Şeyda Acar Broekmans,[1] Astrid Vallès,[1] Ying Poi Liu,[1] Melvin Evers,[1] and Morgane Wartel[1]

[1]Global Research, uniQure biopharma B.V., 1105 BP Amsterdam, the Netherlands

Given that numerous genetic disorders, driven by diverse pathogenic mechanisms, may be amenable to recombinant adeno-associated virus (rAAV)-delivered gene therapies, the sustained innovation of rAAV-based therapeutic modalities is crucial. The progression and severity of genetic diseases can be reduced by targeting the toxic transcripts of a defective gene using microRNA (miRNA)-based miQURE technology delivered within an AAV vector. By adapting the delivered cassette, it may be possible to simultaneously regulate the expression profile of multiple genes involved in the pathogenesis of complex genetic diseases. The established miQURE gene silencing strategy was expanded by concatenating several miQURE molecules in a single construct, resulting in the novel linQURE platform. Here, a proof of mechanism is established by demonstrating that linQURE technology enables the concomitant expression of two synthetic miRNAs *in vitro* and *in vivo*, allowing more efficient downregulation of their disease-causing mRNA targets. This approach supports the development of multi-targeting therapeutic strategies, enabling gene therapy products to adapt to more complex multigenic indications, thus expanding the toolbox of readily available gene therapies.

INTRODUCTION

Developing novel therapeutic approaches for common or rare genetic disorders is a pivotal goal for the biomedical community. The Orphanet database estimates that 72% of identified rare disorders have a cause that should be addressed at the genetic level.[1] This represents hundreds of millions of individuals worldwide who could benefit from newly developed gene therapies. Current therapies are largely palliative, require lifelong treatment, and leave patients with high unmet needs; conversely, gene therapy offers the possibility of a one-time transformative treatment. However, only a limited number of gene therapies have gained US Food and Drug Administration (FDA) or European Medicines Agency (EMA) approvals; seven of these are adeno-associated virus (AAV)-vector-based gene therapies: Glybera (uniQure), Luxturna (Spark Therapeutics), Hemgenix (uniQure/CSL Behring), Roctavian (BioMarin), Zolgensma (Novartis Gene Therapies), Elevidys (Sarepta Therapeutics), and Upstaza (PTC Therapeutics). To date, the AAV-based treatments in clinical practice are gene replacement therapies for monogenic diseases, including inherited retinal disorders (IRDs). IRDs are ideal targets for AAV gene therapy based on ease of access, the immune privilege of the eye, and the existence of novel retina-tropic capsids (ClinicalTrials.gov: NCT02599922, NCT02935517, NCT03316560, and NCT02416622).[2,3] Other approaches, such as targeting the toxic transcripts of a defective gene using a microRNA (miRNA)-based technology, for example, mutant huntingtin in Huntington's disease (HD), have demonstrated safety and efficacy in rodent and minipig models and non-human primates.[4–6] In 2019, the FDA granted fast-track designation, followed by regenerative medicine advanced therapy designation in 2024, to AMT-130, the first one-time-administered gene therapy to enter clinical testing for the treatment of HD. The interim analyses of the ongoing phase 1/2 clinical study for AMT-130 (ClinicalTrials.gov: NCT04120493) show evidence of prospective preserved neurological function with potential dose-dependent clinical benefits for the patients treated with AMT-130, paving the way for a promising future of AAV gene silencing therapies. Most genetic disorders are monogenic; however, the molecular pathogenic mechanisms are often complex, with multiple genes and factors driving the disease phenotype. Evidently, there is a need for highly effective and versatile systems that can target multiple transcripts, expand the toolbox of readily available gene therapies, and offer a cure for more complex genetic disorders. miRNAs constitute a family of ~22-nucleotide (nt)-long RNAs that direct the post-transcriptional repression of target messenger RNAs (mRNAs).[7,8] They are generated from pre-processed forms that enter miRNA maturation pathways for conversion into the final, mature 22 nt miRNA species. The initial form, the primary-miRNA (pri-miRNA), is the direct transcript of the miRNA genomic locus and a substrate of the highly selective microprocessor complex that monitors the presence of specific structural features and nucleotide motifs on all hairpin structures. The microprocessor acts as a gatekeeper, letting only optimal hairpins with miRNA features enter the miRNA biogenesis pathway. It

Received 3 February 2024; accepted 12 August 2024;
https://doi.org/10.1016/j.omtn.2024.102307.

Correspondence: Morgane Wartel, PhD, Global Research, uniQure biopharma B.V., 1105 BP Amsterdam, the Netherlands.
E-mail: m.wartel@uniqure.com

comprises three subunits (Drosha, DGCR8, and SRSF3), each with a defined function and specific hairpin binding motifs.[9] Drosha is the cleaving unit and sits at the hairpin's lower stem. A dimer form of DGCR8 guarantees that Drosha cleaves accurately at the basal junction.[10,11] Finally, SRSF3 promotes microprocessor activity by recruiting Drosha to the basal junction (Figure 1Ai).[10,12] The microprocessor is also sensitive to structural features like internal loops, wobbles, mismatches, apical loop size, and single-stranded RNA segments flanking the hairpin that modulate its propensity to cleave pri-miRNAs.[13–16] Most pri-miRNAs are good microprocessor substrates; however, pri-miR451 is suboptimal (Figure 1B). The miR-451 hairpin possesses poor structural features with a short stem and a loop size of only 4 nt. This affects microprocessor binding and, therefore, miR-451 processing efficiency and expression.[7] pri-miR451 is found in a genomic hairpin cluster close to pri-miR144.[17] pri-miR144 functions as a helper hairpin engaging in cluster assistance and enabling Drosha to process pri-miR451.[7] In short, once pri-miR144 is cleaved by the microprocessor, the microprocessor complex is transferred onto its neighboring pri-miR451, which enables its processing (Figure 1Ai).[18] Once cleaved, both precursor miRNAs (pre-miRNAs) are released in the nucleus and exported to the cytoplasm for processing into mature miRNAs, which ultimately silence their specific transcript targets (Figures 1Aii and 1Aiii). The majority of pre-miRNAs (e.g., pre-miR144) are subjected to a Dicer-dependent canonical miRNA pathway, which leads to guide strand selection and passenger strand degradation within the RNA-induced silencing complex (RISC) before guide-dependent mRNA interference (Figure 1Aii).[19,20] However, pre-miR451 is a notable exception, as it is a poor Dicer substrate.[17] Unlike pri-miR144, pre-miR451 enters a non-canonical Dicer-independent-Ago2-dependent processing pathway, which, following Ago2 slicing, will generate a 30 nt structure that will be progressively 3′ trimmed by the poly(A)-specific ribonuclease (PARN), ultimately generating mature miRNA species of various lengths with no passenger strand (Figure 1Aiii).[21] Thus, the divergent processing pathways utilized by miR144 and miR451 alleviate competition for downstream factors such as Dicer and Ago proteins.[7] Additionally, the absence of a passenger strand from miR451 makes miR144-miR451 the miRNA cluster of choice to efficiently deliver multiple synthetic therapeutic miRNAs while limiting cellular toxicity. This specific feature of the miR144-miR451 cluster was the basis of (1) the modulation of our miQURE 144-451-based proprietary gene silencing platform to enhance single therapeutic miRNA expression from miR451 and (2) the generation of a novel platform, linQURE, to optimally express two therapeutic miRNAs from the cluster. Here, we show the successful modulation of our AAV gene therapy platform and adaptation of the cargo to a multi-expression system and demonstrate its efficacy *in vitro* and *in vivo*.

RESULTS

Optimization of the miR144-miR451 cluster for synthetic miRNA expression

A series of alterations were made to the miR451 and miR144-miR451 scaffolds to further optimize the platform for single-gene targeting and enable multi-gene targeting. As previously described, suboptimal miR451 employs the helper function (represented by the black arrow in Figure 1Ai) of miR144 to enhance its processing and, therefore, the expression of miR451.[7] To demonstrate this, HEK293T cells were transfected with either miR451 alone or miR451 clustered with miR144 (Figure 1C), and RNA was isolated 48 h post-transfection. Small RNA sequencing revealed the augmented expression of a synthetic miRNA from miR451 when it was in a cluster with miR144 (Figure 1Ci); however, another endogenous miRNA, let7a, remained largely unchanged (Figure 1Ciii), suggesting that miR144 and miR451 interact in *cis* (e.g., when miR144 and miR451 are expressed as a cluster on a unique pri-miRNA). Given that the exogenous expression of miR144 may cause unwanted side effects (e.g., the engagement of miR144 targets),[22–24] a novel scaffold modification strategy was implemented to abrogate miR144 expression. Different mutant versions of the miR144 hairpin were engineered, wherein base pairs at positions 5 (miR144M5), 5 and 6 (miR144M56), and 5, 6, and 7 (miR144M567) from the Drosha cleavage site (represented by the black arrowheads in Figure 1D) were mismatched using nucleotide substitutions. The mismatches created a bulge near the Drosha cleavage site, which abrogated processing in precursor forms.[13,14] Each mutant miR144 was clustered with miR451, expressing a synthetic miR-A sequence (Figure 1D, right). As expected, the introduced bulges lowered miR144 expression to varying degrees. The triple mismatch (miR144M567 mutant) reduced expression to undetectable levels (Figure 1Ei). Interestingly, disruption of the Drosha cleavage site in miR144M5 improved miR-A expression from miR451 (Figure 1Eii) as well as miR-A target reporter lowering (Figure 1F), suggesting a mechanism where more Drosha is liberated to process miR451. Notably, disrupting the miR144 hairpin to a greater extent with a double or triple mismatch (miR144M56 and miR144M567 mutants, respectively) did not improve miR-A expression (for miR144M567) or lower reporter expression (for miR144M56 and miR144M567) (Figures 1Eii and 1F). None of the mutants seemed to substantially affect the expression of an endogenous miRNA such as miR16 (Figure 1Eiii).

Therefore, the use of mutant helper miR144 levers miR144-miR451 helper activity without the expression of unwanted miRNAs and, in the case of miR144M5, allows for improved synthetic miRNA expression levels from miR451 and reporter lowering (Figures 1Ei, 1Eii, and 1F). The miR144M5-miR451 cluster was therefore selected and subsequently exploited to develop next-generation linQURE scaffolds.

In vitro validation of a new generation of double-expressing scaffolds, linQURE v.1

Next-generation scaffolds were designed to express multiple synthetic miRNA sequences from one multi-hairpin structure. To this end, various multiplexed versions of miR144M5-miR451 were created and tested for synthetic miRNA expression (Figure 2).

To benefit from optimal miR144M5-451 cluster assistance, the 15 bp miR451 5′ and 3′ flanking regions were conserved, creating a 30 bp spacer sequence between both miR451 hairpins. The human endogenous 92 bp region separating miR144 from miR451 was conserved

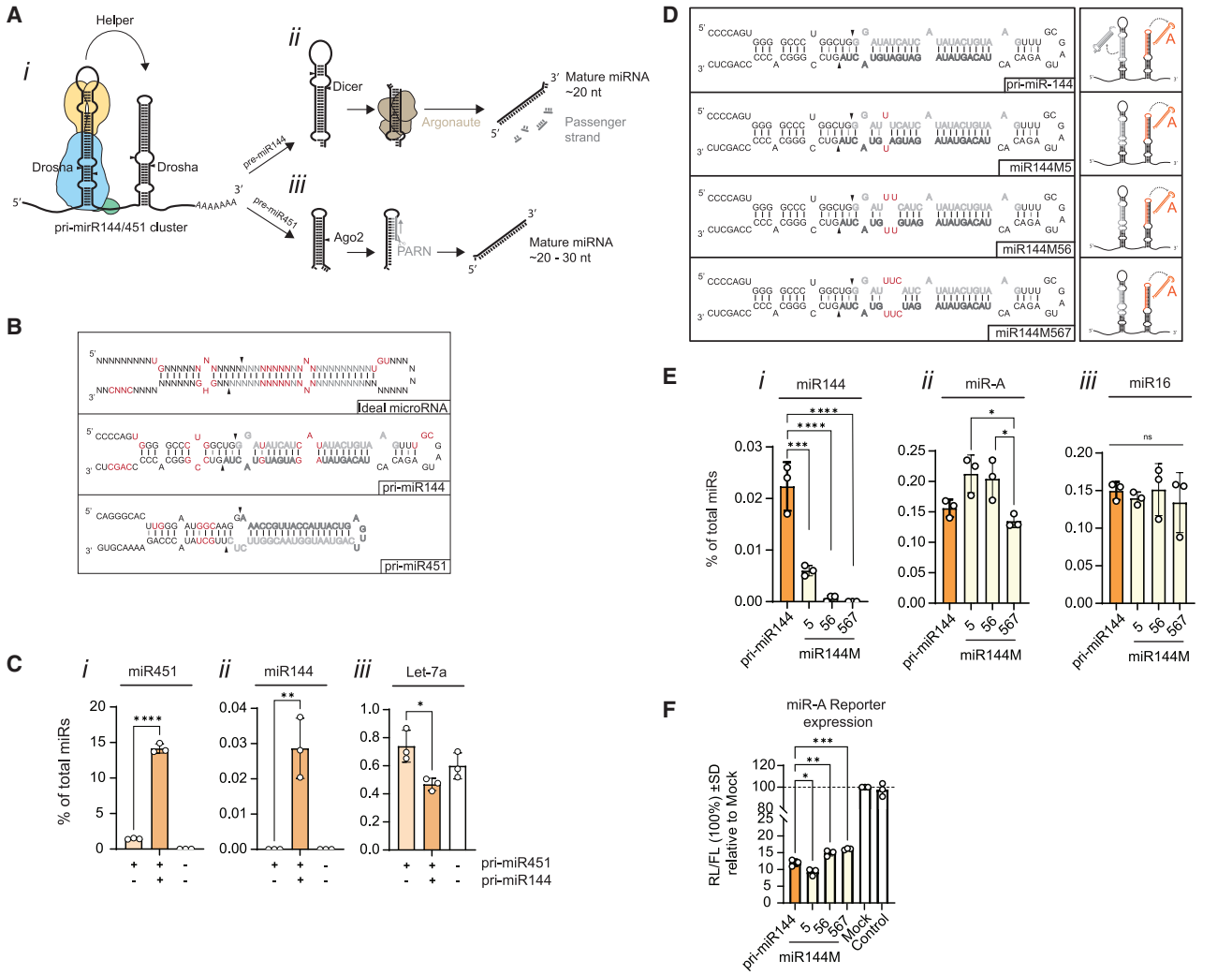

Figure 1. Validation of the miR144-miR451 cluster for synthetic miRNA expression

(Ai) Schematic representation of the processing pathways involved in the maturation of the pri-miR144/451 cluster. The microprocessor is composed of Drosha (blue), a DGCR8 dimer (yellow), and an SRSF3 unit (green). Microprocessor cleavage sites on both hairpins are depicted as black arrowheads. (Aii) While pre-miR144 follows a canonical maturation pathway involving Dicer and the formation of a miRNA duplex, (Aiii) pre-miR451 enters a Dicer-independent pathway involving the slicing and trimming functions of Ago2 and PARN, respectively. This bypasses miRNA duplex formation and leads to a single active guide strand. (B) Depicted hairpins are, from top to bottom, an ideal miRNA hairpin, human miR144, and human miR451. Hairpins are depicted with nucleotide motifs and structural features (in red) that are determinants of microprocessor recognition and cleavage site. Dark gray letters indicate predicted guide strands; light gray letters indicate predicted passenger strands. (C) Comparison of mature miRNA expression from miR451 (Ci) and expression of mature miR144 (Cii) across pri-miR451 and pri-miR144 wild-type/451 scaffolds. miR16 is an endogenous miRNA used as an internal control (Ciii). Quantification was performed by small RNA sequencing on transfected HEK293T cells. Data are presented as mean values (SD) of three technical replicates. Asterisks denote statistically significant differences (*$p \leq 0.05$, **$p \leq 0.01$, and ****$p \leq 0.001$). Student's two-tailed t test was applied for (Ci) and (Cii) and one-way ANOVA followed by Tukey's multiple comparisons test for (Ciii). (D) Depicted hairpins are human pri-miR144 wild type and its mutant variants miR144M5, miR144M56, and miR144M567, with motif modifications highlighted in red. Dark gray letters indicate predicted guide strands, and light gray letters indicate predicted passenger strands. (E) Comparison of mature miR144 (Ei) and mature miR-A (Eii) expression from pri-miR144 wild type and its mutant variants miR144M5, miR144M56, and miR144M567. Endogenous miR16 expression is used as an internal control (Eiii). Quantification was performed by small RNA sequencing on transfected HEK293T cells. Data are presented as mean values (SD) of three technical replicates. Asterisks denote statistically significant differences ($^{ns}p > 0.05$, *$p \leq 0.05$, ***$p \leq 0.005$, and ****$p \leq 0.001$); one-way ANOVA followed by Šídák's or Dunnett's multiple comparisons test. (F) Assessment of knockdown efficiency of miR-A reporter by pri-miR144 wild type and its mutant variants miR144M5, miR144M56, and miR144M567 described in (D). HEK293T cells were co-transfected with the scaffolds and a miR-A luciferase reporter. Data are presented as mean values (SD) of three independent experiments. Asterisks denote statistically significant differences (*$p \leq 0.05$, **$p \leq 0.01$, and ***$p \leq 0.005$); one-way ANOVA followed by Dunnett's multiple comparisons test. FL, firefly luciferase; nt, nucleotides; PARN, poly(A)-specific ribonuclease; RL, Renilla luciferase; SD, standard deviation; ns, not significant.

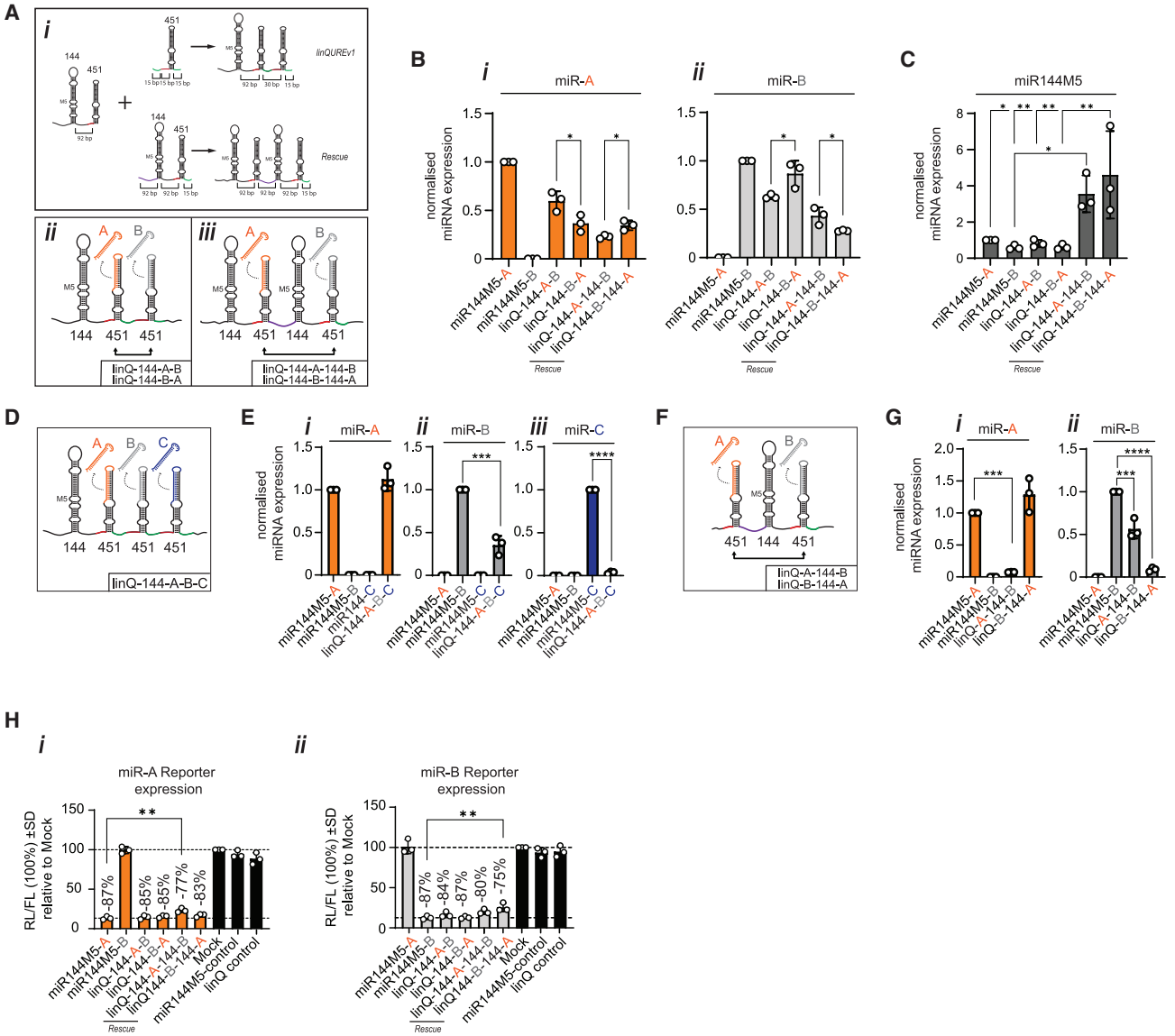

Figure 2. Development of a new generation of double-expressing scaffolds, linQURE v.1

(Ai) Schematic representation of the multiplexing strategy used to create linQURE v.1 scaffolds. Red strand represents the 15 bp 5′ miR451 flanking region; green strand represents the 15 bp 3′ miR451 flanking region conserved to create a 30 bp spacer between both miR451 hairpins. Purple strand represents the linker miR451-miR144 92 bp sequence. (Aii) Schematic representation of the double-expressing miR144M5-miR451-miR451 scaffold expressing miR-A and miR-B (linQ-144-A-B) and (Aiii) schematic representation of a modified double-expressing miR144M5-miR451-miR144M5-miR451 scaffold expressing miR-A and miR-B (linQ-144-A-144-B). Double arrows in (Ai) and (Aii) represent the swapping of miR-A and miR-B positions. (B) Comparison of miR-A (Bi) and miR-B (Bii) expression values across the scaffolds by small RNA sequencing. Data are presented as mean values (SD) of three technical replicates. Asterisks denote statistically significant differences (*$p \leq 0.05$); Student's two-tailed t test. (C) Comparison miR144M5 expression values across the scaffolds by small RNA sequencing. Data are presented as mean values (SD) of three technical replicates. Asterisks denote statistically significant differences (*$p \leq 0.05$ and **$p \leq 0.01$); one-way ANOVA followed by Tukey's multiple comparisons test. (D) Schematic representation of the triple-expressing miR144M5-miR451-miR451-miR451 scaffold expressing miR-A, miR-B, and miR-C (linQ-144-A-B-C). (E) Comparison of miR-A, miR-B, and miR-C expression values across the scaffolds by small RNA sequencing. Data are presented as mean values (SD) of three technical replicates. Asterisks denote statistically significant differences (***$p \leq 0.005$ and ****$p \leq 0.001$); Student's two-tailed t test. (F) Schematic representation of the double-expressing miR451-miR144M5-miR451 scaffold expressing miR-A and miR-B (linQ-A-144-B). (G) Comparison of miR-A (Gi) and miR-B (Gii) expression values across the scaffolds by small RNA sequencing. Data are presented as mean values (SD) of three technical replicates. Asterisks denote statistically significant differences (***$p \leq 0.005$ and ****$p \leq 0.001$); one-way ANOVA followed by Dunnett's multiple comparisons test. (H) Functional validation of the newly developed bi-expressing scaffolds by the Dual-Luciferase assay. The scaffolds were tested for their ability to lower the expression of a miR-A targeted reporter (Hi) and a miR-B targeted reporter (Hii). Data are presented as mean values (SD) of three independent experiments. Asterisks denote statistically significant differences (**$p \leq 0.01$); one-way ANOVA followed by Dunnett's multiple comparisons test. FL, firefly luciferase; miRNA, microRNA; RL, Renilla luciferase; SD, standard deviation.

(Figure 2Ai).[25] To evaluate the impact on expression levels of the integrated miRNA position relative to miR144M5, scaffolds were designed as two derivatives where miR-A and miR-B were placed at a distal or proximal position to the miR144M5 helper (Figure 2Aii). Rescue scaffolds were also designed to evaluate the potential rescue of an additional helper hairpin (Figures 2Ai and 2Aiii), and synthetic miRNA expression across the different scaffold designs was assessed. HEK293T cells were transfected, total RNA was isolated, and small RNA sequencing of total RNA was performed. miR-A and miR-B expression was compared with a single-RNA-expressing counterpart miR144M5-miR451. The quantification data showed a loss of expression for both miR-A (Figure 2Bi) and miR-B (Figure 2Bii) in linQ-144-A-B and linQ-144-B-A, which was more pronounced when the miRNA was integrated within the distal miR451 hairpin (Figure 2B). This loss of expression could not be rescued by the addition of another helper miR144M5 hairpin, which, unexpectedly, further decreased the expression of the first miRNA (Figure 2B). Interestingly, quantification of miR144M5 across scaffolds showed a synergistic effect on expression in the rescue scaffold, suggesting that the helper effect might have been redirected onto the miR144M5 hairpins rather than the miR451 hairpins (Figure 2C). Moreover, the addition of a third miR451 hairpin (miR-C) (Figure 2D) resulted in impaired expression of the second (Figure 2Eii) and third (Figure 2Eiii) integrated miRNAs when compared with single-expressing scaffolds (Figure 2E).

To assess whether a particular localization of helper miR144M5 would improve the expression of both miR451 hairpins, miR144M5 was relocated from its original position (92 bp prior to two miR451 hairpins) to a middle position between two miR451 hairpins at an equal distance (92 bp) from each hairpin. Two derivatives were generated, placing either miR-A or miR-B prior to the miR144M5 helper (Figure 2F), and miR-A (Figure 2Gi) and miR-B (Figure 2Gii) expression was evaluated. Small RNA sequencing results showed a loss of expression of the miRNA located before the miR144M5 helper regardless of the miRNA sequence (Figure 2G), suggesting a role for the spacer sequence separating 144 and 451 in directing the helper activity (e.g., microprocessor transfer) provided by miR144.

To determine the efficiency of miRNA target lowering when expressed from different scaffolds compared with standard scaffolds, plasmids expressing the different scaffolds depicted in Figures 2Aii and 2Aiii were co-transfected along with Dual-Luciferase reporter vectors containing either miR-A or miR-B binding sites in the Renilla luciferase (RL) gene. RL activity was measured by the Dual-Luciferase reporter assay 48 h post-transfection. Both synthetic miRNA sequences miR-A and miR-B within linQ-144-451-451 scaffolds (linQURE v.1) exhibited similar reductions in luciferase reporter expression to those observed when individually expressed within miR144M5-451 standard scaffolds regardless of the more proximal or distal localization from the miR144M5 helper hairpin (Figures 2Hi and 2Hii). Nonetheless, marginally higher reporter gene expression was observed within the rescue scaffolds for both expressed miRNA sequences, with a stronger trend toward the sequence located between two miR144M5 hairpins, in line with miRNA expression data (Figures 2Hi and 2Hii).

Altogether, these data support the use of miR144M5-451-451 to express two synthetic miRNAs and lower two separate targets.

To approximate the gene therapy context, the miR144M5-miR451 (miR144M5-A and miR144M5-B) and linQURE (linQ-144-A-B) scaffolds (Figure 3A) were subcloned within an inverted terminal repeat (ITR) plasmid to enable the subsequent production of AAV9-miR144M5-A, AAV9-miR144M5-B, and AAV9-linQ-144-A-B. Subsequently, HEK293T cells were transduced with a multiplicity of infection (MOI) of 1E+07 genome copies (gc)/cell of either a 1:1 mixture of AAV9-miR144M5-A and AAV9-miR144M5-B or AAV9-linQ-144-A-B alone. Comparable transduction efficiency in all conditions was assessed by vector copy quantification in both test conditions and controls (Figure 3B). For an identical MOI, AAV9-linQ-144-A-B enabled the expression of 3.4 and 2.7 times more miR-A and miR-B, respectively (Figures 3C and 3D), suggesting that linQURE v.1 can be used to deliver multiple engineered miRNAs effectively.

Development of a new generation of double-expressing scaffolds, linQURE v.2

To avoid the structural complexity of the previously described scaffolds and favor optimal miRNA expression, the aim was to employ both the helper capacity of miR144 and its potential as an expressing hairpin (Figure 4A). In contrast to miR451 (a non-canonical, Dicer-independent miRNA), miR144 is processed through a canonical Dicer-dependent pathway.[26,27] Utilizing both miR144 and miR451 simultaneously as expressing scaffolds has the advantage of distributing the maturation of two synthetic miRNAs over two distinct miRNA pathways, therefore optimizing the expression of both mature miRNAs.[28] As a canonical miRNA, miR144 processing generates a miRNA duplex following Drosha and Dicer activity; depending on the relative thermostabilities of the duplex ends, one or the other strand will be favored for RISC loading and mRNA transcript targeting, while the other strand will be degraded (Figure 1Aii).[29] In the case of native miR144, deep sequencing data show that the 3p arm is the guide strand, whereas the 5p arm is degraded (miRBase: hsa-mir-144).

Because the passenger strand selection is sequence dependent, both 5p and 3p regions of miR144 were designed as synthetic miRNA sequence recipients for miR-D (scaffolds linQ D^{5p}-A and linQ D^{3p}-A; Figure 4A). Nucleotide modifications were introduced to adapt miR-D 3p for optimal guide expression (e.g., favor miR-D strand expression; scaffolds linQ D^{3p}M1-A with miR-D ^{19}N>C mutation) or miR-D 3p for optimal passenger expression (e.g., favor miR-D* strand expression; scaffolds linQ D^{3p}M2-A with miR-D ^{1}N>G mutation). The resulting miR-D-expressing scaffolds are shown in Figure 4B.

The expression capacity of miR144 was validated, and the stoichiometries between the guide and passenger strands were determined by

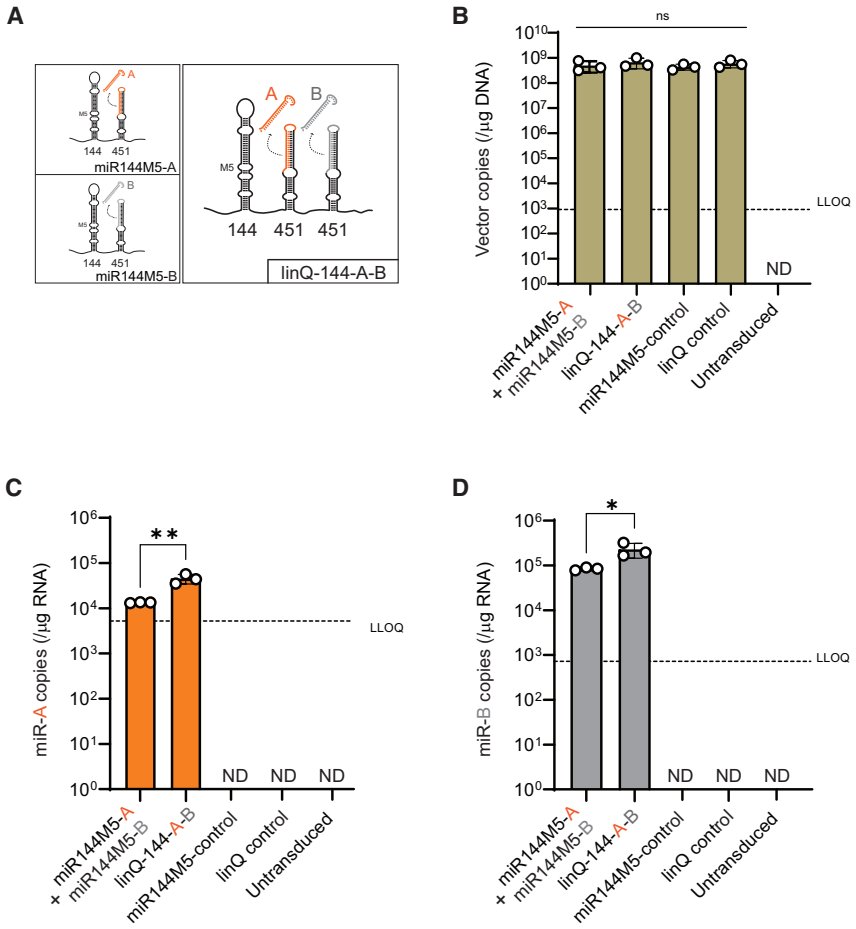

Figure 3. Validation of linQURE v.1 in an AAV9 *in vitro* transduction model

(A) Schematic representation of single-expressing scaffolds miR144M5-miR451 expressing miR-A (miR144M5-A, top left) or miR-B (miR144M5-B, bottom left) vs. the double-expressing miR144M5-miR451-miR451 scaffold expressing miR-A and miR-B (linQ-144-A-B, right panel). (B) Total vector copy expression per transduced sample. (C) Absolute quantification of miR-A copies per µg total RNA per transduced sample. (D) Absolute quantification of miR-B copies per µg total RNA per transduced sample. For (B, C, and D), data are presented as mean values (SD) of three independent experiments; Asterisks denote statistically significant differences ($^{ns}p > 0.05$, $^{*}p \leq 0.05$, and $^{**}p \leq 0.01$); one-way ANOVA followed by Dunnett's multiple comparisons test (A) and unpaired t test (B and C). ND, not detectable; LLOQ, lower limit of quantification; SD, standard deviation; ns, non-significant.

small RNA sequencing and represented as the guide/passenger ratio (G/P ratio) of miR-D over miR-D* (as shown in Figure 4Ci). Scaffold linQ D^{5P}-A had the most favorable G/P ratio (12.4). The nucleotide modification in the scaffold linQ D^{3P}M1-A design increased guide strand expression over the passenger strand, as shown by an increased G/P ratio of 17-fold when compared with the non-modified linQ D^{3P}-A scaffold (5.1 vs. 0.3, respectively). In contrast, the linQ D^{3P}M2-A design had a 7.5-fold lower G/P ratio when compared with linQ D^{3P}-A (0.04 vs. 0.3 respectively), as anticipated, suggesting a predominance of passenger strand expression. Importantly, the guide strand selection modifications in the miR144 hairpin seemed to negatively affect miR-A expression from miR-451 in scaffold linQ D^{3P}M2-A. The most favorable scaffold with respect to miR-A expression was linQ D^{5P}-A (Figure 4Cii).

Following miRNA quantification by small RNA sequencing, the isomiR population (i.e. pool of miRNA variants that differ in length or sequence from the annotated miRNA) for each of the synthetic miRNAs expressed was determined (Figure 4D). Notably, miR-A processing from miR451 was more heterogeneous when compared with miR144-expressed miR-D. The predominantly expressed form was a 25 nt trimmed sequence, which represented over 60% of all miR-A isomiRs with a distribution ranging from 17 to 30 nt trimmed species. The isomiR distribution of miR-A among linQ D^{5P}-A, linQ D^{3P}-A, linQ D^{3P}M1-A, and linQ D^{3P}M2-A was similar, suggesting that the nature of miR144 does not affect the trimming of miR451. In contrast, the processing of miR-D varied greatly among the scaffolds. While scaffold linQ D^{5P}-A produced up to 90% of 23 nt miR-D, scaffold linQ D^{3P}-A produced overall 1-, 2-, or 3-nt-shorter forms of miR-D (22.5%, 55%, and 15.6%, respectively). Interestingly, modifying the G/P ratios also modified the isomiR distribution of miR-D with an increase in the 20 nt isomiR in linQ D^{3P}M1-A and an increase in the 22 nt isomiR in linQ D^{3P}M2-A, suggesting a possible drift of Drosha or Dicer cleavage sites.

Finally, to validate the function of the expressed miRNAs, Dual-Luciferase reporter assays were performed. In brief, plasmids were co-transfected with a Dual-Luciferase reporter vector containing miR-D or miR-A binding sites in the RL gene with a measurement 48 h post-transfection. All scaffolds showed reduced miR-A targeting reporter expression; however, linQ D^{3P}M2-A lowered reporter expression less than other scaffolds (Figure 4Eii), which aligns with the lower miR-A/miR16 ratio observed in Figure 4Cii. The reduced miR-D targeting reporter expression correlated with the G/P ratio, showing a more potent effect from linQ D^{5P}-A (Figure 4Ei).

To validate the use of the double-expressing linQURE v.2 scaffold *in vivo* as a therapeutic modality, a novel scaffold was designed incorporating a set of new synthetic miRNAs: miR-E inserted in miR144 5p and miR-F inserted within miR451 (scaffold linQ E-F) (Figure 5A). *In vitro*, transfection validated the function of linQ E-F, with expression of both synthetic miRNAs (Figure 5Bi) and a G/P ratio of 1.7 (Figure 5Bii). Analysis of the isomiR profiles for both synthetic miRNAs showed a predominance of 23 and 28 nt isomiRs for

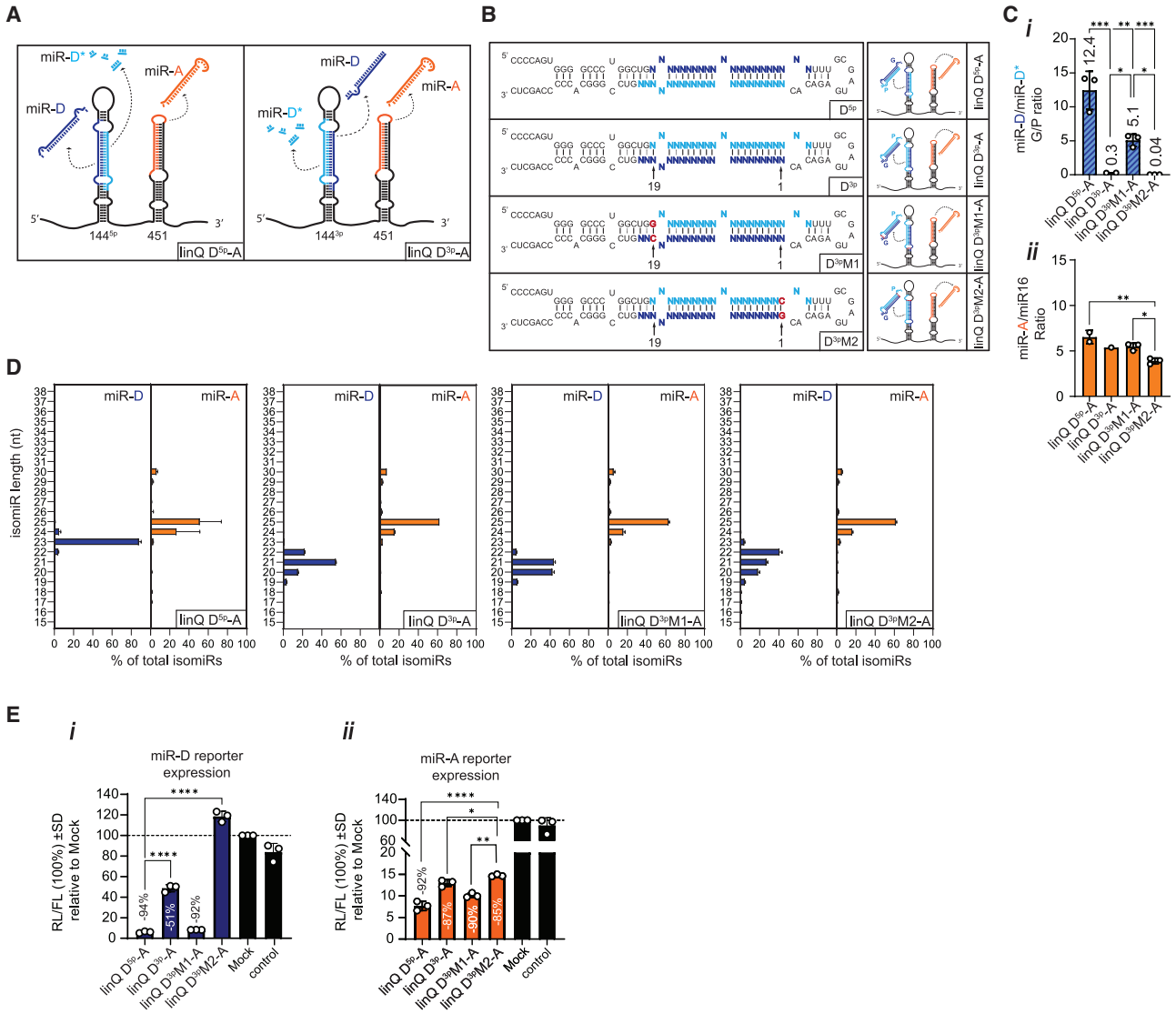

Figure 4. Development of a new generation of double-expressing scaffolds, linQURE v.2

(A) Schematic representation of the double-expressing miR144-5p-miR451 and miR144-3p-miR451 scaffolds expressing miR-D and miR-A (linQ D^{5p}-A and linQD^{3p}-A, respectively). miR144 hairpin expresses a miRNA duplex composed of a guide (miR-D; dark blue) and passenger (miR-D*; light blue) strands. miR451 hairpin expresses a guide strand (miR-A; orange). (B) Depicted hairpins represent human pri-miR144 engineered to express miR-D from 5p arm (D^{5p}) or 3p arm (D^{3p}; D^{3p}M1 and D^{3p}M2) within scaffolds linQ D^{5p}-A, linQD^{3p}-A, linQD^{3p}M1-A, and linQD^{3p}M2-A, respectively. Nucleotide modifications inserted to influence G/P ratios are depicted in red. Dark blue nucleotides indicate inserted synthetic guide strands, light blue nucleotides indicate passenger strands, and black nucleotides indicate the miR144 scaffold sequence. (Ci) Graph compares G/P ratios among linQ D^{5p}-A, linQD^{3p}-A, linQD^{3p}M1-A, and linQD^{3p}M2-A scaffolds. (Cii) Graph represents the expression of miR-A over miR-16 (endogenous control) among linQ D^{5p}-A, linQD^{3p}-A, linQD^{3p}M1-A, and linQD^{3p}M2-A scaffolds. miRNA expression was assessed by small RNA sequencing. Data are presented as mean values (SD) of three technical replicates. Asterisks denote statistically significant differences (*$p \leq 0.05$, **$p \leq 0.005$, and ***$p \leq 0.005$); one-way ANOVA followed by Dunnett's (Ci) or Tukey's (Cii) multiple comparisons test. (D) Analysis of isomiR population for miR-D and miR-A among different scaffolds linQ D^{5p}-A, linQD^{3p}-A, linQD^{3p}M1-A, and linQD^{3p}M2-A. Synthetic miRNA processing was analyzed by small RNA sequencing. Data are presented as mean values (SD) of three technical replicates. (E) Functional validation of the newly developed bi-expressing scaffolds by Dual-Luciferase assay. The scaffolds linQ D^{5p}-A, linQD^{3p}-A, linQD^{3p}M1-A, and linQD^{3p}M2-A were tested for their ability to lower the expression of a miR-D targeted reporter (Ei) and miR-A targeted reporter (Eii). Data are presented as mean values (SD) of three independent experiments. Asterisks denote statistically significant differences (*$p \leq 0.05$, **$p \leq 0.01$, and ****$p \leq 0.001$); one-way ANOVA followed by Dunnett's multiple comparisons test. FL, firefly luciferase; G/P, guide passenger strand ratio; miRNA, microRNA; nt, nucleotides; RL, Renilla luciferase; SD, standard deviation.

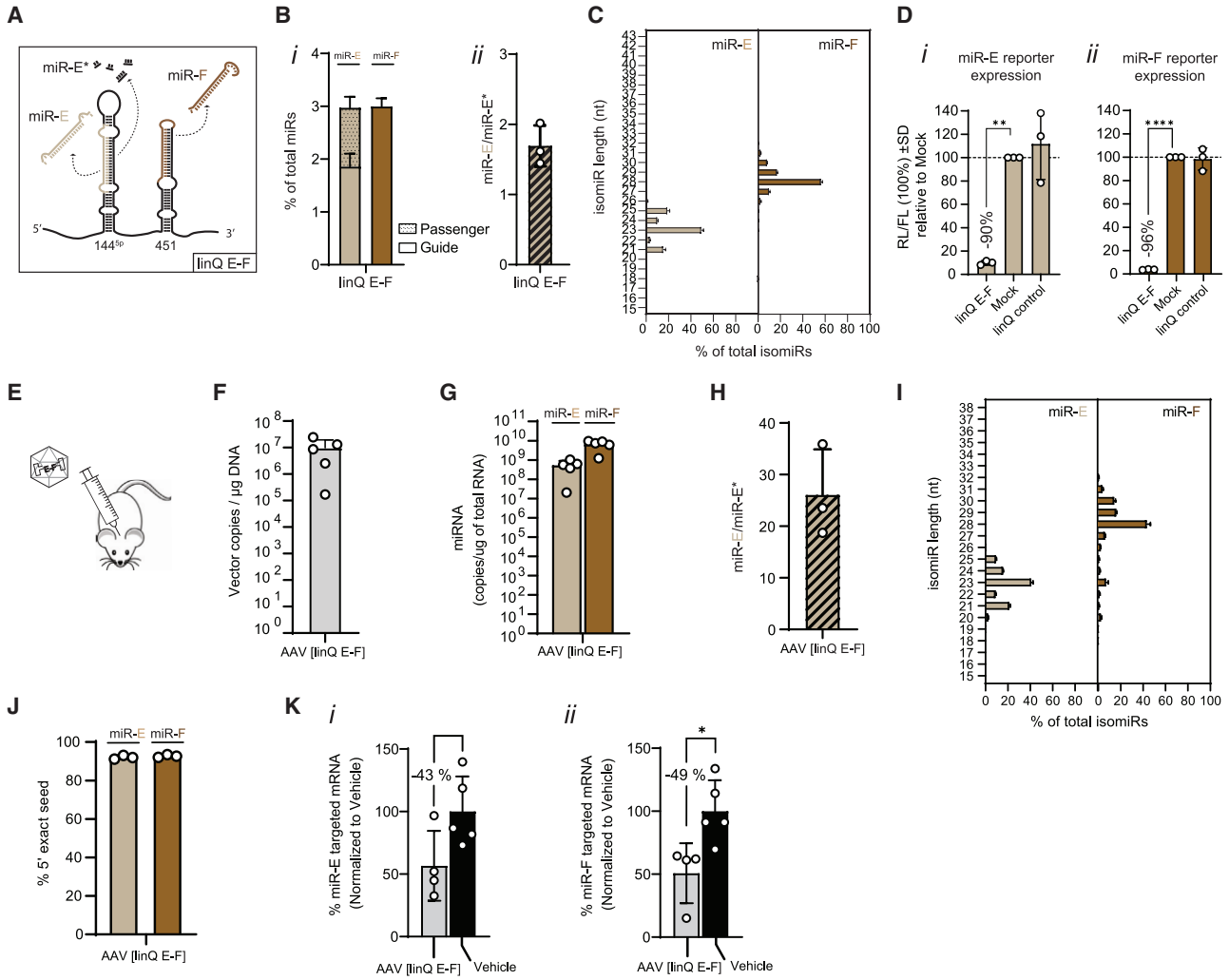

Figure 5. Validation of the miR144-miR451 cluster scaffold linQURE v.2 *in vitro* and *in vivo*

(A) Schematic representation of the double-expressing miR144-5p-miR451 scaffold expressing miR-E and miR-F (linQ E-F). miR144 hairpin expresses a miRNA duplex composed of guide (miR-E; light brown) and passenger (miR-E*; black) strands. miR451 hairpin expresses a guide strand (miR-F; dark brown). (Bi) Graph shows the expression of miR-E guide and passenger strands and miR-F guide strand in transfected HEK293T cells as assessed by small RNA sequencing. Data are presented as mean values (SD) of three technical replicates. (Bii) Graph represents guide (miR-E)/passenger (miR-E*) ratio. Data are presented as mean values (SD) of three technical replicates. (C) Analysis of the isomiR expression of miR-E and miR-F in samples transfected with linQ E-F scaffold. Data are presented as mean values (SD) of three technical replicates. (D) Functional validation of linQ E-F by Dual-Luciferase assay. The scaffold was tested for its ability to lower the expression of a miR-E targeted reporter (Di) and miR-F targeted reporter (Dii). Data are presented as mean values (SD) of three independent experiments. Asterisks denote statistically significant differences (**$p \leq 0.01$, and ****$p \leq 0.001$); one-way ANOVA followed by Dunnett's multiple comparisons test. (E) linQ E-F scaffold was packaged into an AAV5 vector and injected into the striatum of mice. (F) Assessment of transduction efficiency (vector DNA copies) in the striatum of AAV (linQ E-F)-treated mice. Each datapoint represents one animal. Data are represented as mean values (SD); $N = 5$. (G) Absolute quantification of miR-E and miR-F in treated mice by RT-qPCR. Each datapoint represents one animal. Data are represented as mean values (SD); $N = 5$. (H) Assessment of the G/P ratio by small RNA sequencing of the striatum of AAV (linQ E-F)-treated mice. Each datapoint represents one animal. Data are represented as mean values (SD); $N = 3$. (I) Assessment of miR-E and miR-F processing by small RNA sequencing of the striatum of AAV (linQ E-F)-treated mice. Data are represented as mean values (SD); $N = 3$. (J) Quantification of 5′ exact seed processing for miR-E and miR-F guide strands of the striatum of AAV (linQ E-F)-treated mice. Each datapoint represents one animal. Data are represented as mean values (SD); $N = 3$. (K) Quantification of (Ki) miR-E targeted mRNA (normalized to vehicle) and (Kii) miR-F targeted mRNA (normalized to vehicle) of AAV- (linQ E-F) ($N = 4$) and vehicle ($N = 5$)-treated mice. Each datapoint represents one animal. Data are presented as mean values (SD). Asterisks denote statistically significant differences ($^{ns}p > 0.05$ and $^{*}p \leq 0.05$); Student's two-tailed t test. FL, firefly luciferase; miRNA, microRNA; mRNA, messenger RNA; nt, nucleotides; RL, Renilla luciferase; ns, non-significant; SD, standard deviation.

miR-E and miR-F, respectively (Figure 5C). The Dual-Luciferase reporter assay demonstrated the impact of linQ E-F on reporter gene expression *in vitro*, showing 90% and 96% lowering of miR-E and miR-F reporter expression, respectively, when compared with mock control (Figure 5D). To demonstrate *in vivo* validation, linQ E-F was packaged within an AAV5 capsid and delivered to mouse brains

by direct intrastriatal injection (Figure 5E). Mice were sacrificed 12 weeks post-injection, and striatal tissue was collected to evaluate the transduction efficacy and synthetic miRNA expression profiles. For an average of 9.8E+6 vector AAV5 copies/μg striatal deoxyribonucleic acid (DNA) (Figure 5F), miR-E and miR-F expression of 5.2E+8 and 6.6E+9 miRNA copies/μg total RNA, respectively, was achieved (Figure 5G). The miR-E G/P ratio in this context showed a remarkable improvement of 15-fold over the *in vitro* context (26 vs. 1.7, respectively), suggesting a discrepancy in the strand's stability over time *in vivo* (Figure 5H). Importantly, the *in vivo* miRNA processing analysis recapitulated the *in vitro* isomiR profiles of both synthetic miRNAs (Figure 5I) with more than 95% of exact 5′ seed sequence expression (Figure 5J), suggesting an extreme Drosha fidelity to generate active miRNA species. Finally, quantification of the miR-E (Figure 5Ki) and miR-F (Figure 5Kii) target transcripts showed reduced expression of 43% and 49%, respectively, when compared with vehicle-treated mice. Taken together, the miRNA expression data and functional assays demonstrate that (1) two distinct synthetic miRNAs can be expressed from one scaffold *in vitro* and *in vivo*; (2) modifying the miR144 sequence does not affect its helper function toward miR451; (3) synthetic miRNA expression of both 3p and 5p from miR144 can lead to optimal target lowering; (4) modulation of the G/P ratio can be achieved, which enriches the desired strand; and (5) requisite expression of both synthetic miRNAs expressed from miR144 and miR451 can be achieved *in vivo* following local AAV injection.

DISCUSSION

It was nearly 50 years ago that gene therapy was initially proposed as a means of treating inherited monogenic disorders. Since then, significant progress has been made in the field, with more than 20 gene therapies approved for clinical application.[30] These approvals offer life-changing treatment options for diseases previously deemed untreatable or unresponsive to traditional therapies. Gene supplementation is becoming an established strategy to treat monogenic disorders that benefit from the exogenous delivery of a functional protein-coding gene, such as the AAV-based gene therapies Zolgensma for treating spinal muscular atrophy and Hemgenix for hemophilia B.[31–33] Following successful clinical trials, there has been a resurgence of interest in using RNA interference (RNAi)—encompassing small interfering RNA (siRNA) and short hairpin RNA (shRNA)/miRNA strategies—to tackle complex multi-factorial disorders using gene silencing products for diseases such as hepatitis C, liver and kidney dysfunction, neurologic disorders, and various cancers.[34] However, optimally treating diseases driven by multiple dysregulated pathways cannot be achieved with a mono-target therapy. The concept of multi-targeting is established in pharmacology, notably for oncology indications where combinations of small-molecule inhibitors are expected to become the standard of care.[35] In order to expand the clinical outreach of miRNA gene therapies, combined silencing of multiple genes must be explored. Furthermore, given that a single mismatch between an miRNA and its target sequence will affect the silencing potency of the therapy,[36] the genetic variation caused by single-nucleotide polymorphisms (SNPs) may limit the population-wide application of miRNA therapies. Thus, expressing multiple miRNAs with distinct binding sites toward the same target could overcome the inherent barrier caused by SNPs.[36,37]

The current study builds upon the well-established AAV-miQURE platform[4,6,38–43] by optimizing its single therapeutic miRNA expression and enabling the expression of two therapeutic miRNAs from one cassette. Different silencing approaches were evaluated using the synchronized expression of artificial miRNAs. The miRNA cluster was successfully modulated and adapted to a multi-expression system, which demonstrated efficacy *in vitro* and *in vivo*.

The miQURE platform utilizes the non-canonical miRNA hairpin miR451 to mitigate the risk of passenger-dependent off targeting. miR451 is an Ago2-dependent Dicer-independent miRNA, which makes it a scaffold of choice for therapeutic tools. However, miR451 is structurally suboptimal, which limits its conversion into therapeutic miRNA. We and others have shown that combining miR451 with its endogenously occurring miRNA partner miR144 substantially potentiates miR451 processing and, ultimately, benefits therapeutic translation.[18,44] Here, we used informed engineering to enable miRNA processing to be turned on and off. miR144 Drosha processing was transferred toward miR451 by introducing a single point mutation translated to a bulge in the lower stem of miR144. This likely precluded miR144 from being processed by Drosha while maintaining its recruitment capacity.[13] However, it increased miR451 processing and its functional effect. A pivotal location was identified within the structure of miR144, where Drosha recruitment was gradually lost when the bulge was doubled and tripled, modulating the helper function of the canonical hairpin.[45,46]

To harness this unique feature of miR451, a multi-expression system was engineered by adding a second miR451 hairpin (linQURE v.1). Although the system enabled proper miRNA expression, the levels of the second miR451 were lower regardless of the inserted synthetic sequence. Furthermore, the system did not allow successful clustering of a third miR451, suggesting that cluster assistance requires the presence of more than one canonical hairpin to function effectively. Indeed, we observed preferential cluster assistance between canonical and canonical, rather than canonical and non-canonical, hairpin pairings.[18] These data are corroborated by others who have shown that expression is limited if the cluster is expanded even in the sole presence of a canonical hairpin, which may be due to the limited availability of Drosha to pursue the processing of all hairpins.[45,46]

Overall, our findings and those of others suggest that a canonical hairpin benefits the optimal expression of multiple miRNAs. Therefore, linQURE v.2 was developed, wherein miR144 was converted to an expressor, which enabled the required G/P ratio control. RNAi toxicity can be mediated by elevated passenger strand production and saturation of the RNAi machinery.[47,48] An advantage of the linQURE v.2 system is that an alternate processing pathway is used,

which avoids saturation of the Dicer/Ago pathways and alleviates the possibility of competitive processing.[49] Additionally, the miRNA backbone was optimized for guide expression, which, importantly, was conserved *in vivo*.

Ultimately, the construct design strategy will be informed by its intended use. For example, a particular disease indication may favor selecting multiple targets over the magnitude of transcript repression, or vice versa. In some cases, it may be desirable to direct maximal efficacy toward one target (e.g., a target with no deleterious effects when silenced) and less in another (where safety concerns arise if excessive suppression occurs). These data suggest that using informed design would allow miRNA expression to be optimally modulated for specific disease indications.

Product improvements can be made to develop a gene therapy product that maximizes miRNA expression while preserving patient safety (e.g., minimal off-target activity and avoiding high AAV doses), such as optimizing the processing and, therefore, the expression of therapeutic miRNAs. The future lies in the *de novo* design of semi-artificial miRNAs that incorporate all essential optimal processing motifs, thus ensuring more efficient and accurate processing than any other natural pri-miRNA, in conjunction with combined off-target assessments of the multiple miRNAs.[11,13,15,16,50–52] Another barrier to multi-targeting technologies lies upstream with the selection of several strategic targets that broadly aim to perturb pathobiological mechanisms rather than focusing on single targets.[53–55] Despite the evaluation of multi-targeting with siRNA/shRNA technologies, these therapies have not achieved successful clinical translation.[56,57] Associating a multi-expression platform such as linQURE with the properties of an AAV vector enables the controlled delivery of multiple transgenes, which may solve potential regulatory concerns on the path to the clinic.

In conclusion, the linQURE platform is well adapted to address the current need for multi-targeting options required to expand the gene therapy toolbox.

MATERIALS AND METHODS

Expression cassettes: Design and cloning

In total, six miRs (designated miR-A to -F) and the miR-control (non-targeting miRNA) guide and complementary strands were embedded into the human pri-miR451 or pri-miR144 sequences. The miR451 scaffold and the pri-miR144/451 scaffold were flanked by 157 and 28 nt 5′ flanking regions, respectively. All scaffolds were flanked by a 205 nt 3′ flanking region followed by a BamHI restriction site and a poly(A) signal. Each association of hairpins comprised a spacer sequence that separated the first and second hairpins. miR144 and miR451 were separated by a 92 bp spacer sequence, miR451 and miR144 were separated by the reversed 92 bp spacer sequence, and miR451 and miR451 were separated by a synthetic 30 bp spacer sequence.

NheI and NotI restriction sites were added at the 5′ and 3′ ends, respectively, and the complete sequence was synthesized and subcloned into a pUC vector (GeneWiz, Azenta Life Sciences, Guangzhou, China). Expression from all cassettes was driven by a strong synthetic ubiquitous promoter. The cassettes comprising miR144-miR451 scaffolds (and variants) (Figure 1), linQURE scaffolds linQ-A-144-B, linQ-144-A-B, linQ-144-A-B-C, and linQ-144-A-144-B (Figure 2), and linQ-D-A and its variants (Figure 4) were terminated by the bovine growth hormone poly(A) signal. Cassettes comprising the linQURE scaffold linQ E-F (Figure 5) were terminated by the simian virus-40 poly(A) signal. For AAV plasmid generation, the previously synthesized expression cassettes miR144M5-A, miR144M5-B, miR144M5-control, linQ-144-A-B, linQ control, and linQ E-F, including the promoter and poly(A) signal, were incorporated in a plasmid encoding the AAV ITR. ITR plasmid subcloning and sequence verification were performed by GeneWiz (Azenta Life Sciences, Leipzig, Germany).

AAV vectors

AAV5 vectors

Recombinant AAV5 constructs were produced by polyethylenimine transfection of HEK293T cells with two plasmids encoding for Rep-Cap and the ITR-containing transgene plasmid (Sirion Biotech, PerkinElmer, Gräfelfing, Germany). Following a two-step purification using POROS CaptureSelect AAV-X resin (Thermo Fisher Scientific, Waltham, MA) for primary capture and an iodixanol gradient (Sirion Biotech, PerkinElmer, Gräfelfing, Germany) for empty capsid removal. The titer of the purified AAV was determined using quantitative polymerase chain reaction (qPCR).

AAV9 vectors

AAV9 vectors harboring the expression cassettes were produced by infecting expressSF+ insect cells (Protein Sciences, Meriden, CT) with two baculoviruses, one encoding Rep and Cap and the other encoding the transgene. AAV preparations were purified by a fast protein liquid chromatography AKTA Pure system (Cytiva Life Sciences, Marlborough, MA) that employed an AAV-X affinity resin (Thermo Fisher Scientific), with an ultrafiltration step using a 100 kDa filter to exchange buffer to vehicle buffer. AAV titers were determined using qPCR.

Animal studies

The mouse study was approved by the central governmental committee for animal experimentation and the animal welfare body of the Netherlands Organization for Applied Scientific Research in compliance with European Community specifications regarding the use of laboratory animals. The study was conducted by Charles River Laboratories (Charles River Laboratories, Kuopio, Finland), which are accredited by the Association for Assessment and Accreditation of Laboratory Animal Care.

To determine the *in vivo* expression of linQ E-F, AAV5 vectors were generated encoding scaffold linQ E-F as previously described. A cohort of 5 (female and male) mice were injected intrastriatally with 1.5E+11 gc/hemisphere. Weekly body weight measurements and cage-side observations were made until 20 weeks of age (12 weeks post-infusion)when the mice were euthanized. Striatal samples were

collected, snap frozen, and used to extract DNA for vector genome quantification and RNA for miR-E and miR-F quantification by RT-qPCR and processing analysis by small RNA sequencing. DNA and RNA were isolated using the AllPrep DNA/RNA 96-well kit (Qiagen, Venlo, the Netherlands) as per the manufacturer's instructions.

Culture, transfection, and transduction of HEK293T cells

HEK293T cells were maintained in Dulbecco's modified Eagle's medium (Thermo Fisher Scientific) containing heat-inactivated fetal bovine serum (Thermo Fisher Scientific) at 37°C and 5% CO_2. For transfection and transduction assays, cells were seeded in 96- or 24-well plates at a density of 2E+04 or 1E+05 cells/well, respectively, 1 day prior to transfection or transduction. Cells were either transfected with 0.05, 0.5, or 1 pg/cell in triplicate or transduced with AAV9 vectors at an MOI of 1E+07 total gc/cell in duplicate. Two days post-transfection/transduction, the cells were harvested, and genomic DNA and total RNA were isolated according to the manufacturer's instructions (AllPrep DNA/RNA Micro Kit, Qiagen) for subsequent molecular analysis.

Molecular analysis of *in vitro* and *in vivo* samples

Quantification of vector copies

Vector genome copies from isolated genomic DNA were quantified by TaqMan qPCR assay (Thermo Fisher Scientific) and qualified standard lines. qPCR was performed on 7500 Fast Real-Time PCR System (Thermo Fisher Scientific) and analyzed on 7500 Software (v.2.3) (Thermo Fisher Scientific).

Quantification of miRNA copies

To quantify the expression of synthetic miR-A, miR-B, miR-E, and miR-F from total RNA, miRNA-specific assays were developed. In brief, to detect synthetic miRNA expression levels, isolated RNA was reverse transcribed into cDNA by using either a TaqMan MicroRNA Reverse Transcription Kit (Cat. #4366597, Applied Biosystems, Waltham, MA) or Maxima First Strand cDNA Synthesis Kit with a dsDNAse step (Cat. #K1672, Thermo Fisher Scientific) and a gene-specific reverse transcriptase primer to target the synthetic miRNA. cDNA was quantified by using TaqMan qPCR assays (Custom TaqMan Small RNA Assay miR-A assay ID CSYPDRM and Custom TaqMan Small RNA Assay miR-B assay ID CT2W72H) and SYBR Green qPCR assays (miR-F_23 nt-FW: 5′-AGACAGACTTGCTTAAAGGAAG-3′, miR-F_23 nt-RV: 5′-GGTCCAGTTTTTTTTTTTTTTTACAC-3′; miR-E_23 nt-FW: 5′-CAGTCAGGTCTTTTCTTGTTCA-3′, miR-E_23 nt-RV: 5′-CCAGTTTTTTTTTTTTTTTTCGGGT-3′, Thermo Fisher Scientific) and qualified standard lines. The qPCR was performed on 7500 Fast Real-Time PCR System (Thermo Fisher Scientific) and analyzed on 7500 Software (v.2.3) (Thermo Fisher Scientific).

Quantification of target mRNA copies

To quantify mRNA expression from total RNA, mRNA-specific assays were developed. In brief, isolated RNA was reverse transcribed into cDNA by using either Maxima First Strand cDNA Synthesis Kit with a dsDNAse step (Cat. #K1672, Thermo Fisher Scientific) or SuperScript III First-Strand Synthesis System (Cat. #18080051, Thermo Fisher Scientific). cDNA was quantified using TaqMan qPCR assays (E-targeted mRNA assay: Pr-FW: 5′-AGGGTGAACAAGAAAAGA CCTG-3′, Pr-RV: 5′-CGGTTGTTTCCCTCCTTGTTTT-3′, probe: [FAM] 5′-TAAAGATTAACCAGAAG-3′ [NFQ-MGB] [Eurofins Scientific, Luxemburg, Luxemburg]; F-targeted mRNA Assay: Pr-FW: 5′-CGACTGGAGCACGAGGACACTGA-3′, Pr-RV: 5′-CACCCAGCT TCGGTCAGAG-3′, Probe: [FAM] 5′-CGGGTAGAA/ZEN/GCGGG GGCTCT/3IABkFQ-3′) and qualified standard lines. The qPCR was performed on 7500 Fast Real-Time PCR System (Thermo Fisher Scientific) and analyzed on 7500 Software (v.2.3) (Thermo Fisher Scientific).

Dual-Luciferase reporter assay

To assess reporter gene lowering by Dual-Luciferase reporter assay (Promega, Madison, Wisconsin), HEK293T cells were plated into 96- or 24-well tissue-culture-treated plates at a density of 2E+04 or 1E+05 cells/well, respectively. Plasmid DNA (pDNA) (0.05, 0.5, or 1 pg/cell) was co-transfected with Dual-Luciferase target-specific reporters using Lipofectamine 2000 (Thermo Fisher Scientific). The co-transfection was performed at a 1:2, 5:1, or 6:1 pDNA:reporter ratio. The reporters contain relevant miRNA binding in the 3′ UTR of the RL gene and a herpes simplex virus type 1 thymidine kinase-driven firefly luciferase (FL). The RL and FL activity was measured by Dual-Luciferase reporter assay 48 h post-transfection. Reporter lowering was measured as a decrease in the RL/FL activity ratio. All transfections were performed as technical triplicates. The assay readouts were acquired in a GloMax Microplate Reader (Promega). The experiments were performed two or three times.

Small RNA sequencing using next-generation sequencing and data analysis

Total RNA was isolated from transfected HEK293T cells as described above. Small RNA sequencing was performed by GenomeScan BV (Leiden, the Netherlands) using the NebNext small RNA library prep method (*in vitro* samples) or the NextFlex small RNA library preparation method (*in vivo* samples), including BluePippin size selection of the final library combined with Illumina NovaSeq6000 PE150 sequencing. The data were delivered and analyzed in-house using CLC Genomics Workbench Suite v.20 (Qiagen). The trimmed small RNA reads were aligned against the human or mouse database of miRNAs (miRbase v.22) and a custom database containing the synthetic (pre-)miRNA sequences. The quantification of miR-A to -F, miR144 and variants, and endogenous miR16 (guide and passenger strands where relevant) were expressed as a percentage of the number of counts vs. the total number of small RNA counts.

DATA AND CODE AVAILABILITY

Materials and reagents commercially procured will be shared upon request. Reagents such as the AAV vectors generated by the authors will not be shared unless a memorandum of understanding is signed between the research-sponsoring institution and the requester. Methods are available to disclose, and all data associated with this study are present within the manuscript.

ACKNOWLEDGMENTS

This study was funded by uniQure biopharma B.V., Amsterdam, the Netherlands. We thank Sebastian Kieper, PhD, for his scientific contributions; Kristel van Rooijen and

Anna-Aster de Ruiter, PhD, for their help with experiments; Leontien van der Bent, PhD, and Rhodé Erbrink, PhD, for their help with bioinformatic analyses; Stephane Baudouin, PhD, for his help with statistical analysis; and Richard Porter, PhD for his constructive criticism of the manuscript. The authors thank Julia Jenkins, PhD, of GK Pharmacomm, Ltd., for providing medical writing support/editorial support, which was funded by uniQure biopharma B.V. in accordance with Good Publication Practice (GPP3) guidelines (http://www.ismpp.org/gpp3).

AUTHOR CONTRIBUTIONS

I.B., M.W., V.Z., Y.P.L., S.A.B., and A.V. conceived and designed the experiments. M.E. gave scientific input. Experiments were performed by I.B., A.M.G., S.K., and P.d.M.H., and data were analyzed by I.B. and V.Z. I.B., A.M.G., S.K., and P.d.M.H. contributed to the preparation of reagents, materials, and analytical tools. All authors provided critical revisions of the manuscript, provided final approval prior to submission, and agreed to be accountable for the work.

DECLARATION OF INTERESTS

I.B., M.W., V.Z., Y.P.L., S.A.B., A.V., and M.E. are uniQure employees, hold uniQure stocks, and are inventors on the corresponding patent applications. A.M.G., S.K., and P.d.M.H. are uniQure employees and hold uniQure stocks.

REFERENCES

1. Nguengang Wakap, S., Lambert, D.M., Olry, A., Rodwell, C., Gueydan, C., Lanneau, V., Murphy, D., Le Cam, Y., and Rath, A. (2020). Estimating cumulative point prevalence of rare diseases: analysis of the Orphanet database. Eur. J. Hum. Genet. *28*, 165–173. https://doi.org/10.1038/s41431-019-0508-0.

2. Hu, M.L., Edwards, T.L., O'Hare, F., Hickey, D.G., Wang, J.-H., Liu, Z., and Ayton, L.N. (2021). Gene therapy for inherited retinal diseases: progress and possibilities. Clin. Exp. Optom. *104*, 444–454. https://doi.org/10.1080/08164622.2021.1880863.

3. Tian, X., Zheng, Q., Xie, J., Zhou, Q., Liang, L., Xu, G., Chen, H., Ling, C., and Lu, D. (2023). Improved gene therapy for MFRP deficiency-mediated retinal degeneration by knocking down endogenous bicistronic Mfrp and Ctrp5 transcript. Mol. Ther. Nucleic Acids *32*, 843–856. https://doi.org/10.1016/j.omtn.2023.05.001.

4. Spronck, E.A., Brouwers, C.C., Vallès, A., de Haan, M., Petry, H., van Deventer, S.J., Konstantinova, P., and Evers, M.M. (2019). AAV5-miHTT Gene Therapy Demonstrates Sustained Huntingtin Lowering and Functional Improvement in Huntington Disease Mouse Models. Mol. Ther. Methods Clin. Dev. *13*, 334–343. https://doi.org/10.1016/j.omtm.2019.03.002.

5. Spronck, E.A., Vallès, A., Lampen, M.H., Montenegro-Miranda, P.S., Keskin, S., Heijink, L., Evers, M.M., Petry, H., van Deventer, S.J., Konstantinova, P., et al. (2021). Intrastriatal Administration of AAV5-miHTT in Non-Human Primates and Rats Is Well Tolerated and Results in miHTT Transgene Expression in Key Areas of Huntington Disease Pathology. Brain Sci. *11*, 129. https://doi.org/10.3390/brainsci11020129.

6. Vallès, A., Evers, M.M., Stam, A., Sogorb-Gonzalez, M., Brouwers, C., Vendrell-Tornero, C., Acar-Broekmans, S., Paerels, L., Klima, J., Bohuslavova, B., et al. (2021). Widespread and sustained target engagement in Huntington's disease minipigs upon intrastriatal microRNA-based gene therapy. Sci. Transl. Med. *13*, eabb8920. https://doi.org/10.1126/scitranslmed.abb8920.

7. Fang, W., and Bartel, D.P. (2020). MicroRNA Clustering Assists Processing of Suboptimal MicroRNA Hairpins through the Action of the ERH Protein. Mol. Cell *78*, 289–302.e6. https://doi.org/10.1016/j.molcel.2020.01.026.

8. Bofill-De Ros, X., and Vang Ørom, U.A. (2024). Recent progress in miRNA biogenesis and decay. RNA Biol. *21*, 1–8. https://doi.org/10.1080/15476286.2023.2288741.

9. Nguyen, T.A., Jo, M.H., Choi, Y.-G., Park, J., Kwon, S.C., Hohng, S., Kim, V.N., and Woo, J.-S. (2015). Functional Anatomy of the Human Microprocessor. Cell *161*, 1374–1387. https://doi.org/10.1016/j.cell.2015.05.010.

10. Auyeung, V.C., Ulitsky, I., McGeary, S.E., and Bartel, D.P. (2013). Beyond secondary structure: primary-sequence determinants license pri-miRNA hairpins for processing. Cell *152*, 844–858. https://doi.org/10.1016/j.cell.2013.01.031.

11. Dang, T.L., Le, C.T., Le, M.N., Nguyen, T.D., Nguyen, T.L., Bao, S., Li, S., and Nguyen, T.A. (2020). Select amino acids in DGCR8 are essential for the UGU-pri-miRNA interaction and processing. Commun. Biol. *3*, 344. https://doi.org/10.1038/s42003-020-1071-5.

12. Kim, K., Nguyen, T.D., Li, S., and Nguyen, T.A. (2018). SRSF3 recruits DROSHA to the basal junction of primary microRNAs. RNA *24*, 892–898. https://doi.org/10.1261/rna.065862.118.

13. Li, S., Nguyen, T.D., Nguyen, T.L., and Nguyen, T.A. (2020). Mismatched and wobble base pairs govern primary microRNA processing by human Microprocessor. Nat. Commun. *11*, 1926. https://doi.org/10.1038/s41467-020-15674-2.

14. Li, S., Le, T.N.-Y., Nguyen, T.D., Trinh, T.A., and Nguyen, T.A. (2021). Bulges control pri-miRNA processing in a position and strand-dependent manner. RNA Biol. *18*, 1716–1726. https://doi.org/10.1080/15476286.2020.1868139.

15. Nguyen, T.L., Nguyen, T.D., Bao, S., Li, S., and Nguyen, T.A. (2020). The internal loops in the lower stem of primary microRNA transcripts facilitate single cleavage of human Microprocessor. Nucleic Acids Res. *48*, 2579–2593. https://doi.org/10.1093/nar/gkaa018.

16. Roden, C., Gaillard, J., Kanoria, S., Rennie, W., Barish, S., Cheng, J., Pan, W., Liu, J., Cotsapas, C., Ding, Y., and Lu, J. (2017). Novel determinants of mammalian primary microRNA processing revealed by systematic evaluation of hairpin-containing transcripts and human genetic variation. Genome Res. *27*, 374–384. https://doi.org/10.1101/gr.208900.116.

17. Yang, J.-S., Maurin, T., Robine, N., Rasmussen, K.D., Jeffrey, K.L., Chandwani, R., Papapetrou, E.P., Sadelain, M., O'Carroll, D., and Lai, E.C. (2010). Conserved vertebrate mir-451 provides a platform for Dicer-independent, Ago2-mediated microRNA biogenesis. Proc. Natl. Acad. Sci. USA *107*, 15163–15168. https://doi.org/10.1073/pnas.1006432107.

18. Shang, R., Baek, S.C., Kim, K., Kim, B., Kim, V.N., and Lai, E.C. (2020). Genomic Clustering Facilitates Nuclear Processing of Suboptimal Pri-miRNA Loci. Mol. Cell *78*, 303–316.e4. https://doi.org/10.1016/j.molcel.2020.02.009.

19. Hutvágner, G., McLachlan, J., Pasquinelli, A.E., Bálint, E., Tuschl, T., and Zamore, P.D. (2001). A cellular function for the RNA-interference enzyme Dicer in the maturation of the let-7 small temporal RNA. Science *293*, 834–838. https://doi.org/10.1126/science.1062961.

20. Ketting, R.F., Fischer, S.E., Bernstein, E., Sijen, T., Hannon, G.J., and Plasterk, R.H. (2001). Dicer functions in RNA interference and in synthesis of small RNA involved in developmental timing in C. elegans. Genes Dev. *15*, 2654–2659. https://doi.org/10.1101/gad.927801.

21. Yang, J.-S., and Lai, E.C. (2010). Dicer-independent, Ago2-mediated microRNA biogenesis in vertebrates. Cell Cycle *9*, 4455–4460. https://doi.org/10.4161/cc.9.22.13958.

22. Huang, X., Chao, R., Zhang, Y., Wang, P., Gong, X., Liang, D., and Wang, Y. (2021). CAP1, a target of miR-144/451, negatively regulates erythroid differentiation and enucleation. J. Cell Mol. Med. *25*, 2377–2389. https://doi.org/10.1111/jcmm.16067.

23. Li, H., Zhou, J., Wei, X., Chen, R., Geng, J., Zheng, R., Chai, J., Li, F., and Jiang, S. (2016). miR-144 and targets, c-fos and cyclooxygenase-2 (COX2), modulate synthesis of PGE2 in the amnion during pregnancy and labor. Sci. Rep. *6*, 27914. https://doi.org/10.1038/srep27914.

24. Lin, W., Tang, Y., Zhao, Y., Zhao, J., Zhang, L., Wei, W., and Chen, J. (2020). MiR-144-3p Targets FoxO1 to Reduce Its Regulation of Adiponectin and Promote Adipogenesis. Front. Genet. *11*, 603144. https://doi.org/10.3389/fgene.2020.603144.

25. Choi, J.-G., Bharaj, P., Abraham, S., Ma, H., Yi, G., Ye, C., Dang, Y., Manjunath, N., Wu, H., and Shankar, P. (2015). Multiplexing seven miRNA-Based shRNAs to suppress HIV replication. Mol. Ther. *23*, 310–320. https://doi.org/10.1038/mt.2014.205.

26. Cheloufi, S., Dos Santos, C.O., Chong, M.M.W., and Hannon, G.J. (2010). A dicer-independent miRNA biogenesis pathway that requires Ago catalysis. Nature *465*, 584–589. https://doi.org/10.1038/nature09092.

27. Cifuentes, D., Xue, H., Taylor, D.W., Patnode, H., Mishima, Y., Cheloufi, S., Ma, E., Mane, S., Hannon, G.J., Lawson, N.D., et al. (2010). A novel miRNA processing pathway independent of Dicer requires Argonaute2 catalytic activity. Science *328*, 1694–1698. https://doi.org/10.1126/science.1190809.

28. Ma, H., Zhang, J., and Wu, H. (2014). Designing Ago2-specific siRNA/shRNA to Avoid Competition with Endogenous miRNAs. Mol. Ther. Nucleic Acids *3*, e176. https://doi.org/10.1038/mtna.2014.27.

29. Medley, J.C., Panzade, G., and Zinovyeva, A.Y. (2021). microRNA strand selection: Unwinding the rules. Wiley Interdiscip. Rev. RNA *12*, e1627. https://doi.org/10.1002/wrna.1627.

30. Arabi, F., Mansouri, V., and Ahmadbeigi, N. (2022). Gene therapy clinical trials, where do we go? An overview. Biomed. Pharmacother. *153*, 113324. https://doi.org/10.1016/j.biopha.2022.113324.

31. Keeler, A.M., and Flotte, T.R. (2019). Recombinant Adeno-Associated Virus Gene Therapy in Light of Luxturna (and Zolgensma and Glybera): Where Are We, and How Did We Get Here? Annu. Rev. Virol. *6*, 601–621. https://doi.org/10.1146/annurev-virology-092818-015530.

32. Pipe, S.W., Leebeek, F.W.G., Recht, M., Key, N.S., Castaman, G., Miesbach, W., Lattimore, S., Peerlinck, K., Van der Valk, P., Coppens, M., et al. (2023). Gene Therapy with Etranacogene Dezaparvovec for Hemophilia B. N. Engl. J. Med. *388*, 706–718. https://doi.org/10.1056/NEJMoa2211644.

33. Shah, J., Kim, H., Sivamurthy, K., Monahan, P.E., and Fries, M. (2023). Comprehensive analysis and prediction of long-term durability of factor IX activity following etranacogene dezaparvovec gene therapy in the treatment of hemophilia B. Curr. Med. Res. Opin. *39*, 227–237. https://doi.org/10.1080/03007995.2022.2133492.

34. Traber, G.M., and Yu, A.-M. (2023). RNAi-Based Therapeutics and Novel RNA Bioengineering Technologies. J. Pharmacol. Exp. Ther. *384*, 133–154. https://doi.org/10.1124/jpet.122.001234.

35. Zhong, L., Li, Y., Xiong, L., Wang, W., Wu, M., Yuan, T., Yang, W., Tian, C., Miao, Z., Wang, T., and Yang, S. (2021). Small molecules in targeted cancer therapy: advances, challenges, and future perspectives. Sig Transduct Target Ther *6*, 201–248. https://doi.org/10.1038/s41392-021-00572-w.

36. Moszyńska, A., Gebert, M., Collawn, J.F., and Bartoszewski, R. (2017). SNPs in microRNA target sites and their potential role in human disease. Open Biol. *7*, 170019. https://doi.org/10.1098/rsob.170019.

37. Gebert, M., Jaśkiewicz, M., Moszyńska, A., Collawn, J.F., and Bartoszewski, R. (2020). The Effects of Single Nucleotide Polymorphisms in Cancer RNAi Therapies. Cancers *12*, 3119. https://doi.org/10.3390/cancers12113119.

38. Zancanella, V., Vallès, A., Liefhebber, J.M.P., Paerels, L., Tornero, C.V., Wattimury, H., van der Zon, T., van Rooijen, K., Golinska, M., Grevelink, T., et al. (2023). Proof-of-concept study for liver-directed miQURE technology in a dyslipidemic mouse model. Mol. Ther. Nucleic Acids *32*, 454–467. https://doi.org/10.1016/j.omtn.2023.04.004.

39. Miniarikova, J., Zanella, I., Huseinovic, A., van der Zon, T., Hanemaaijer, E., Martier, R., Koornneef, A., Southwell, A.L., Hayden, M.R., van Deventer, S.J., et al. (2016). Design, Characterization, and Lead Selection of Therapeutic miRNAs Targeting Huntingtin for Development of Gene Therapy for Huntington's Disease. Mol. Ther. Nucleic Acids *5*, e297. https://doi.org/10.1038/mtna.2016.7.

40. Keskin, S., Brouwers, C.C., Sogorb-Gonzalez, M., Martier, R., Depla, J.A., Vallès, A., van Deventer, S.J., Konstantinova, P., and Evers, M.M. (2019). AAV5-miHTT Lowers Huntingtin mRNA and Protein without Off-Target Effects in Patient-Derived Neuronal Cultures and Astrocytes. Mol. Ther. Methods Clin. Dev. *15*, 275–284. https://doi.org/10.1016/j.omtm.2019.09.010.

41. Evers, M.M., Miniarikova, J., Juhas, S., Vallès, A., Bohuslavova, B., Juhasova, J., Skalnikova, H.K., Vodicka, P., Valekova, I., Brouwers, C., et al. (2018). AAV5-miHTT Gene Therapy Demonstrates Broad Distribution and Strong Human Mutant Huntingtin Lowering in a Huntington's Disease Minipig Model. Mol. Ther. *26*, 2163–2177. https://doi.org/10.1016/j.ymthe.2018.06.021.

42. Miniarikova, J., Zimmer, V., Martier, R., Brouwers, C.C., Pythoud, C., Richetin, K., Rey, M., Lubelski, J., Evers, M.M., van Deventer, S.J., et al. (2017). AAV5-miHTT gene therapy demonstrates suppression of mutant huntingtin aggregation and neuronal dysfunction in a rat model of Huntington's disease. Gene Ther. *24*, 630–639. https://doi.org/10.1038/gt.2017.71.

43. Reilmann, R., Ross, C., Testa, C., Frank, S., Evers, M., de Haan, M., Valles-Sanchez, A., Konstantinova, P., van Deventer, S., and Higgins, J. (2020). Translation of AMT-130 Preclinical Data to Inform the Design of the First FDA-approved Human AAV Gene Therapy Clinical Trial in Adults with Early Manifest Huntington's Disease (4531). Neurology *94*. https://www.neurology.org/doi/10.1212/WNL.94.15_supplement.4531.

44. Kretov, D.A., Walawalkar, I.A., Mora-Martin, A., Shafik, A.M., Moxon, S., and Cifuentes, D. (2020). Ago2-Dependent Processing Allows miR-451 to Evade the Global MicroRNA Turnover Elicited during Erythropoiesis. Mol. Cell *78*, 317–328.e6. https://doi.org/10.1016/j.molcel.2020.02.020.

45. Bhaskaran, V., Nowicki, M.O., Idriss, M., Jimenez, M.A., Lugli, G., Hayes, J.L., Mahmoud, A.B., Zane, R.E., Passaro, C., Ligon, K.L., et al. (2019). The functional synergism of microRNA clustering provides therapeutically relevant epigenetic interference in glioblastoma. Nat. Commun. *10*, 442. https://doi.org/10.1038/s41467-019-08390-z.

46. Bhaskaran, V., Yao, Y., Bei, F., and Peruzzi, P. (2019). Engineering, delivery, and biological validation of artificial microRNA clusters for gene therapy applications. Nat. Protoc. *14*, 3538–3553. https://doi.org/10.1038/s41596-019-0241-8.

47. Grimm, D., Streetz, K.L., Jopling, C.L., Storm, T.A., Pandey, K., Davis, C.R., Marion, P., Salazar, F., and Kay, M.A. (2006). Fatality in mice due to oversaturation of cellular microRNA/short hairpin RNA pathways. Nature *441*, 537–541. https://doi.org/10.1038/nature04791.

48. Grimm, D., Wang, L., Lee, J.S., Schürmann, N., Gu, S., Börner, K., Storm, T.A., and Kay, M.A. (2010). Argonaute proteins are key determinants of RNAi efficacy, toxicity, and persistence in the adult mouse liver. J. Clin. Invest. *120*, 3106–3119. https://doi.org/10.1172/JCI43565.

49. McBride, J.L., Boudreau, R.L., Harper, S.Q., Staber, P.D., Monteys, A.M., Martins, I., Gilmore, B.L., Burstein, H., Peluso, R.W., Polisky, B., et al. (2008). Artificial miRNAs mitigate shRNA-mediated toxicity in the brain: Implications for the therapeutic development of RNAi. Proc. Natl. Acad. Sci. USA *105*, 5868–5873. https://doi.org/10.1073/pnas.0801775105.

50. Fang, W., and Bartel, D.P. (2015). The Menu of Features that Define Primary MicroRNAs and Enable De Novo Design of MicroRNA Genes. Mol. Cell *60*, 131–145. https://doi.org/10.1016/j.molcel.2015.08.015.

51. Kwon, S.C., Baek, S.C., Choi, Y.-G., Yang, J., Lee, Y.-S., Woo, J.-S., and Kim, V.N. (2019). Molecular Basis for the Single-Nucleotide Precision of Primary microRNA Processing. Mol. Cell *73*, 505–518.e5. https://doi.org/10.1016/j.molcel.2018.11.005.

52. Galka-Marciniak, P., Olejniczak, M., Starega-Roslan, J., Szczesniak, M.W., Makalowska, I., and Krzyzosiak, W.J. (2016). siRNA release from pri-miRNA scaffolds is controlled by the sequence and structure of RNA. Biochim. Biophys. Acta *1859*, 639–649. https://doi.org/10.1016/j.bbagrm.2016.02.014.

53. Li, C., Zhang, X., Cheng, L., Dai, L., Xu, F., Zhang, J., Tian, H., Chen, X., Shi, G., Li, Y., et al. (2013). RNA interference targeting human FAK and EGFR suppresses human non-small-cell lung cancer xenograft growth in nude mice. Cancer Gene Ther. *20*, 101–108. https://doi.org/10.1038/cgt.2012.91.

54. Malek, A., Gyorffy, B., Catapano, C.V., and Schäfer, R. (2013). Selection of optimal combinations of target genes for therapeutic multi-gene silencing based on miRNA co-regulation. Cancer Gene Ther. *20*, 326–329. https://doi.org/10.1038/cgt.2013.20.

55. Shahzad, M.M.K., Lu, C., Lee, J.-W., Stone, R.L., Mitra, R., Mangala, L.S., Lu, Y., Baggerly, K.A., Danes, C.G., Nick, A.M., et al. (2009). Dual targeting of EphA2 and FAK in ovarian carcinoma. Cancer Biol. Ther. *8*, 1027–1034. https://doi.org/10.4161/cbt.8.11.8523.

56. Jai, J., Shirleen, D., Hanbali, C., Wijaya, P., Anginan, T.B., Husada, W., and Pratama, M.Y. (2022). Multiplexed shRNA-miRs as a candidate for anti HIV-1 therapy: strategies, challenges, and future potential. J. Genet. Eng. Biotechnol. *20*, 172. https://doi.org/10.1186/s43141-022-00451-z.

57. Michael, F.M., Chandran, P., Chandramohan, K., Iyer, K., Jayaraj, K., Sundaramoorthy, R., and Venkatachalam, S. (2019). Prospects of siRNA cocktails as tools for modifying multiple gene targets in the injured spinal cord. Exp. Biol. Med. *244*, 1096–1110. https://doi.org/10.1177/1535370219871868.